The *in vivo* mechanics of the magnetotactic backbone as revealed by correlative FLIM-FRET and STED microscopy

Erika Günther[1], *André Klaußz*[2,4], *Mauricio Toro-Nahuelpan*[3,5], *Dirk Schüler*[3], *Carsten Hille*[2,6], *Damien Faivre*[1,7,*]

[1]Department of Biomaterials, Max Planck Institute of Colloids and Interfaces, Science Park Golm, 14424 Potsdam, Germany

[2]Physical Chemistry, Institute of Chemistry, University of Potsdam, 14476 Potsdam, Germany

[3]Department of Microbiology, University Bayreuth, 95447 Bayreuth, Germany

[4]Present address: *HOLOEYE* Photonics AG, 12489 Berlin, Germany

[5]Present address: European Molecular Biology Laboratory, 69117 Heidelberg, Germany

[6]Present address: Technical University of Applied Sciences Wildau, 15745 Wildau, Germany

[7]Aix Marseille University, CEA, CNRS, BIAM, 13108 Saint Paul-Lez-Durance, France

[*] **e-mail: damien.faivre@mpikg.mpg.de.**

Supplementary information

Control experiments

We acquired two consecutive FLIM-FRET and STED images of the same cells. First, we verified changes in distance between MamJ-phiYFP and TagRFP657-MamK using FLIM-FRET and in the structure of the filament of TagRFP657-MamK by STED microscopy. The bacteria are embedded in an agarose matrix to keep them alive, but also to prevent them from being able to freely move and in particular rotate. We performed FLIM-FRET and STED microscopy on a bacterium and after 20 min regeneration period, the same procedure was repeated on the same cell. Supplementary Figure 2a shows the STED image of three cells (TagRFP675-MamK filaments). Supplementary Figure 2b shows the identical cells after 20 min regeneration period. Both images display consistent and straight filaments.

In addition, using equation (1), we calculated the FRET efficiency at the beginning of the experiment $E = 78 \pm 5\%$ (n = 14 cells, N = 10 images, 2 independent experiments / imaging of different cultures and at different days). After 20 min regeneration period, the FRET efficiency is $E = 82 \pm 3\%$ (n = 13 cells, N = 10 images, 2 independent experiments). The calculated distance between the donor phiYFP and acceptor TagRFP657 using equation (4) is $r = 3.7 \pm 0.2$ nm (n = 14, N = 10) and $r = 3.4 \pm 0.2$ nm (n = 13, N = 10) for the repeated measurement after 20 min. The FLIM-FRET results demonstrate that the distance of MamJ-phiYFP and TagRFP657-MamK change slightly during STED imaging and the 20 min regeneration period in a range of $\Delta r = 0.3$ nm, which is statistically significant ($P < 0.01$), but physiologically not relevant. Additionally, the STED images of the TagRFP657-MamK filament are similar (see also Supplementary Figure S2).

Measured fluorescence decay times, calculated FRET efficiencies and donor-acceptor distances

We measured the fluorescence decay time (τ) of the donor phiYFP in presence and absence of the acceptor TagRFP657 by time-correlated single-photon counting (TCSPC). Decay curves from MamJ-phiYFP strains were successfully fitted (χ_R^2 = 1.28) to a single-exponential decay function with a resulting decay time τ_D = 2.95 ns. Decay curves of MamJ-phiYFP + TagRFP657-MamK strains show a faster decay compared to the MamJ-phiYFP strains. We quantified this decay behavior by a bi-exponential decay function (χ_R^2 = 1.10), determining the interacting and non-interacting donor populations, resulting in a second decay time τ_{DA} = 0.56 ns (with a fixed decay time τ_D = 2.94 ns). Supplementary Tab. 1 summarizes the calculated fluorescence decay times of the donor phiYFP of different MSR-1 strains and statistical analysis. No significant change is observed between the fluorescence decay times τ_D of MamJ-phiYFP and phiYFP + TagRFP657-MamK constructs. Thus, the presence of donor and acceptor fluorescent proteins alone is not sufficient for FRET events. However, in the presence of donor and acceptor fluorescent proteins fused to MamJ and MamK, the fluorescence decay times decrease significantly, but independent of the mechanical treatment (see also Supplementary Tab. 1).

Energy transfer between MamJ-phiYFP and TagRFP657-MamK

MamJ-phiYFP + TagRFP657-MamK was excited up to 4 times longer than MamJ-phiYFP or phiYFP + TagRFP657 to get sufficient counts for analyzing, indicating the successful energy transfer from the donor (phiYFP) in presence of the acceptor (TagRFP657). On the other hand, direct acceptor excitation with the same power at 635 nm did not result in increased acceptor

intensity in MamJ-phiYFP + TagRFP657-MamK due to the low quantum yield (0.1) of TagRFP657.

Fitting procedure

When applying time-resolved donor fluorescence measurements for studying FRET interactions, the measurements provide access to non-interacting and interacting fractions of the donor molecules – a benefit compared to intensity-based FRET recordings. Thus, the standard procedure is then divided into two steps[1]. First, the donor fluorescence decay time is recorded alone (τ_D) and subsequently in the presence of the acceptor (τ_D). Figure 1a shows the mono-exponential decay behavior of the donor alone (yielding τ_D with χ_R^2-values of 1.28, Supplementary Fig. S11). In the presence of donor and acceptor without interaction (control), the donor decay is not changed (still mono-exponential decay behavior), indicating the absence of influence of the fluorescent acceptor on the donor (see Supplementary Tab. S3, second row, added Supplementary Fig. S14).

However, in the case of a possible interaction between donor and acceptor, we clearly saw a multi-exponential donor fluorescence decay behavior (see Figure 1, Supplementary Fig. S14). Since we only detected donor molecules, the simplest way was to assume non-interacting and interacting donor molecules. Since non-interacting donor exhibited a mono-exponential decay time of 2.95 ns (which did not change under the presence of non-interaction acceptor), we fixed this value (only the time component, but not the fractional contribution). The second time component then corresponded to the interacting donor with reduced decay time originating from the energy transfer to the acceptor. Thus, bi-exponential decay fitting with only one fixed time component resulted then in the second time component (indicating the FRET efficiency) and in the fractional contribution (indicating the amount of interacting donor relative to all available donor molecules).

The determined IRF value (460 ps) falls within common range for this type of experimental setup (and is mainly determined by the SPAD-detector timing[2]. Theoretically, temporal resolutions down to 1/10 of the IRF can be reached, but in practice values of ½ of the IRF are realistic and distinguishable[3]. Thus, the time components we obtained could be analyzed with sufficient accuracy. In addition, the residuals and χ_R^2-values indicated a reliable fitting procedure.

Autofluorescence contribution

A significant fluorescence signal under the chosen experimental conditions could not be observed in cells lacking the donor or acceptor (Supplementary Fig. S1c, e). Thus, autofluorescence was neglected.

STED microscopy on MamK filaments

After one STED round, we observed a certain structure, but the image had an insufficient quality (in term of counts). Accordingly, we waited 20 min in order to compare two consecutive STED images/ filaments. In the interval, the structure is likely reformed since, after 20 min of regeneration time, we observed again a fluorescence signal. We hypothesized the new fluorescent filament originated from treadmilling. We therefore concluded that the cells were still alive and that no significant phototoxicity took place.

High FRET efficiencies, collection of photons

Supplementary Tab. S3 shows that approximately 73 % to 81 % are interacting donor molecules. In general, not all donor molecules are able to interact with the acceptor[1]. However, upon the presence of a dynamic and intact MamK filament, or a stiff and static filament, the MamJ turnover remains constant[4]. Consequently, the dynamic behavior of MamJ is independent of MamK and is

proposed to only transiently interact with MamK. The half time of recovery of MamJ fusion proteins after photobleaching is approximately 10 s [4] and thus indicates a transient MamJ-MamK interaction < 20 s [4]. All photons were collected in an image obtained within approximately 50 s for the fluorescence decay fitting in the FLIM-FRET analysis, since faster point and line scans resulted in insufficient photon statistics. Consequently, short time interactions are averaged out for numerical FRET analysis. However, during the scanning process, interacting and non-interacting donor populations were visualized. On the one hand, free MamJ and MamK in the cytoplasm could result in this occurrence. On the other hand, under the assumption that the MamJ-MamK interactions are < 20 s, an inhomogeneous decay time distribution in a FLIM image recorded within 50 s could be considered. Hence, this distribution would reflect the non-synchronized and transient interaction in a bacterium, as observed in the presented results.

Normalization of TagRFP657 fluorescence intensities

The images were normalized to maximum count value for comparison. Indeed, the counts refer as arbitrary unit to the recorded fluorescence intensity per pixel (Figure 4c: 0 - 84 counts per pixel, normalized to 84 counts = 1). Nevertheless, the changed intensities did not totally refer to bleaching, but also to slight changes in position and / or focus, to changed protein expression and/ or distribution, and to variations due to the microscope setup, since we measured in sub-diffraction space. Still, the counts were high enough to produce a meaningful image.

Plasmid construction

Plasmids were constructed by amplifying the DNA fragments of interest with the Phusion High Fidelity DNA Polymerase (Thermo Scientific). Plasmid description and oligonucleotides are listed

in Supplementary Tab. 5 to 7, respectively (see below). Plasmids were introduced into *M. gryphiswaldense* by conjugation.

To generate pMT092, the *phiYFP* gene (Evrogen) was amplified with the oligonucleotides oMTN292 and oMTN293. Subsequently, the *phiYFP* fragment was *Hind*III-*Bam*HI digested and ligated into the identically digested pMT082 vector.

To construct pMT093, the *TagRFP657* (Addgene) gene was amplified (oMTN294-295) and further cloned into the vector pMT080 under the control of the *mamAB* operon promoter (P_{mamAB}) using the restriction sites *Nde*I-*Eco*RI.

Plasmid pMT094 was created by amplifying the *mamK* gene (oMTN045-296) and subsequently cloned into pMT093 by using the *Hind*III-*Bam*HI restriction sites.

For creation of pMT095, the *TagRFP657-mamK* fragment was amplified (oMTN297-298) and *Bam*HI-*Xho*I digested to be cloned into identically digested pMT092 vector.

For construction of pMT107, the *phiYFP* + *TagRFP657-mamK* fragment was amplified (oMTN353-355) and cloned into pMT094 using the *Nde*I-*Bam*HI restriction sites.

Finally, to construct pMT108, the vector pMT107 was *Bam*HI-*Xho*I digested. Subsequently, blunt ends were generated and further re-ligated (in addition see Supplementary Tab. 5 - 7).

The fusions MamJ-phiYFP, TagRFP657-MamK, and MamJ-phiYFP + TagRFP657-MamK rescued the phenotypes of the Δ*mamJ*, Δ*mamK, and* Δ*mamJK* strains, respectively, which exhibited wild type-like magnetosomes chains (data not shown). This means that the fusions are functional.

Supplementary figures

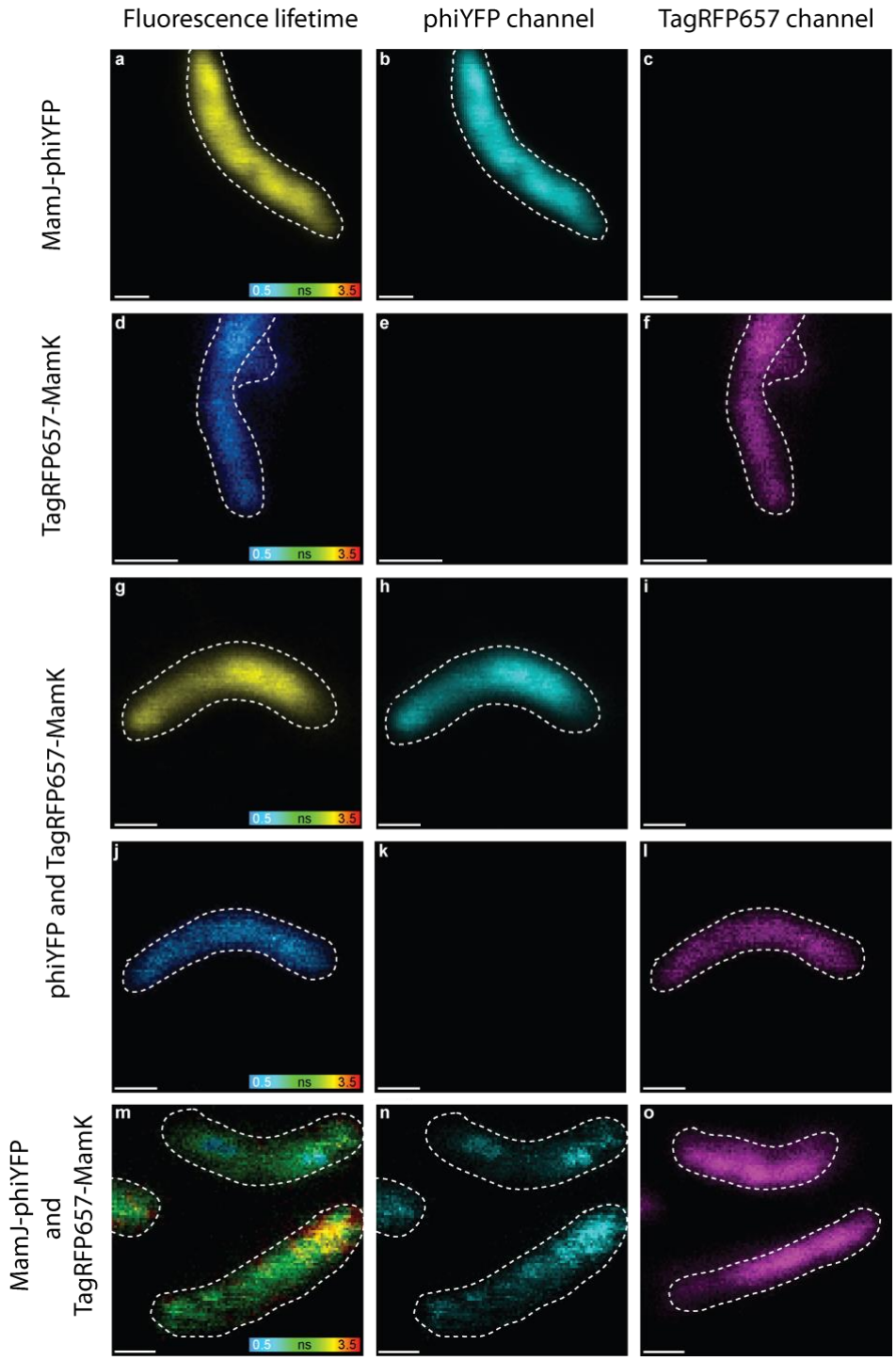

Supplementary Figure S1**: Fluorescence lifetime and fluorescence intensity images of MamJ-phiYFP, TagRFP657-MamK and MamJ-phiYFP + TagRFP657-MamK in the phiYFP**

channel and TagRFP657 channel. The first row shows MSR-1 cells with only MamJ-phiYFP (a-c) with the fluorescence lifetime image of the phiYFP-channel colored in yellow (a) indicating a long donor decay time. The fluorescence intensity image is colored in cyan (b). The second row illustrates MSR-1 cells with only TagRFP657-MamK (d-f) with the fluorescence lifetime image of the TagRFP657-channel colored in blue (d) indicating a short acceptor decay time. The fluorescence intensity image is colored in purple (f). The third and fourth row shows MSR-1 cells with TagRFP657-MamK and phiYFP (g-l) with the fluorescence lifetime image of the phiYFP-channel colored in yellow (g) indicating a long donor decay time and with the fluorescence lifetime image of the TagRFP657-channel colored in blue (j) indicating a short acceptor decay time. The fluorescence intensity of phiYFP is colored in cyan (h) and the fluorescence intensity of TagRFP657 is colored in purple (l). The fifth row shows MSR-1 cells with MamJ-phiYFP and TagRFP657-MamK (m-o) with the fluorescence lifetime image of the phiYFP-channel (m), in which green colors indicate the reduced donor decay time due to energy transfer. The fluorescence intensity of phiYFP is colored in cyan (n) and the fluorescence intensity of TagRFP657 is colored in purple (o).

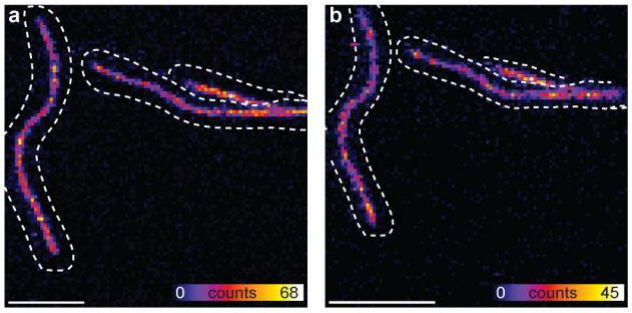

Supplementary Figure S2: **STED images of MSR-1 cells expressing MamJ-phiYFP + TagRFP657-MamK.** The fluorescence intensity of TagRFP657 was recorded, indicating the filament TagRFP657-MamK. First image scan (a) second image scan after 20 min regeneration period (b). Scale bar: 1 µm.

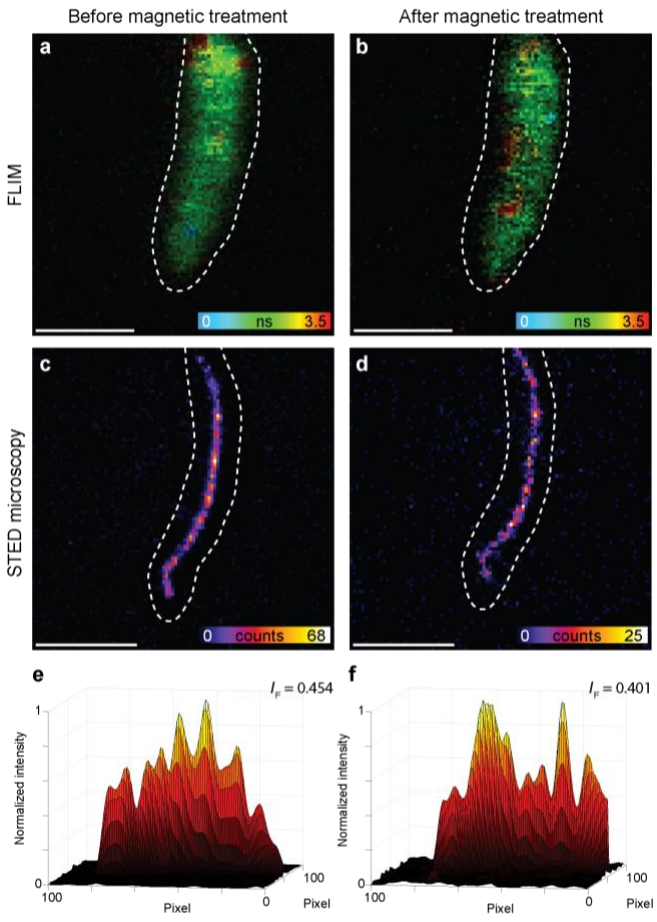

177

178 Supplementary Figure S3: ***In vivo*** **FLIM-FRET and STED experiments on MSR-1 cells before**
179 **and after magnetic field rotation.** FLIM images (a, b) and STED images (c, d) of MSR-1 cells
180 with MamJ-phiYFP + TagRFP657-MamK before (a, c) and after (b, d) applying a magnetic field.
181 (e, f) Corresponding 3D surface intensity plots of the STED images. For a better illustration, we
182 normalized the intensity and used a Gaussian filter.

183

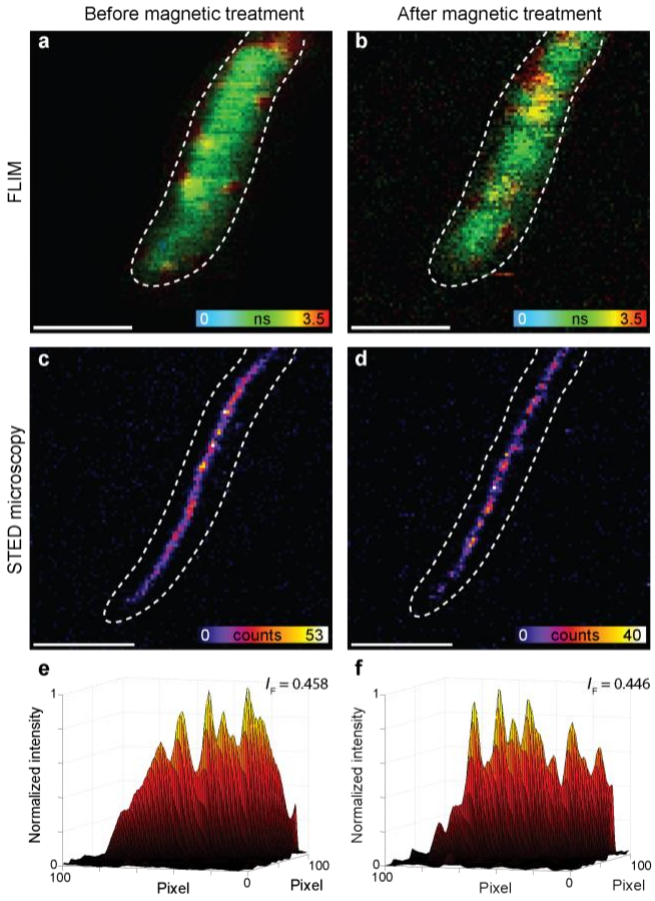

184

185 Supplementary Figure S4: ***In vivo*** **FLIM-FRET and STED experiments on MSR-1 cells before**
186 **and after magnetic field rotation.** FLIM images (a, b) and STED images (c, d) of MSR-1 cells
187 with MamJ-phiYFP + TagRFP657-MamK before (a, c) and after (b, d) applying a magnetic field.
188 (e, f) Corresponding 3D surface intensity plots of the STED images. For a better illustration, we
189 normalized the intensity and used a Gaussian filter.

190

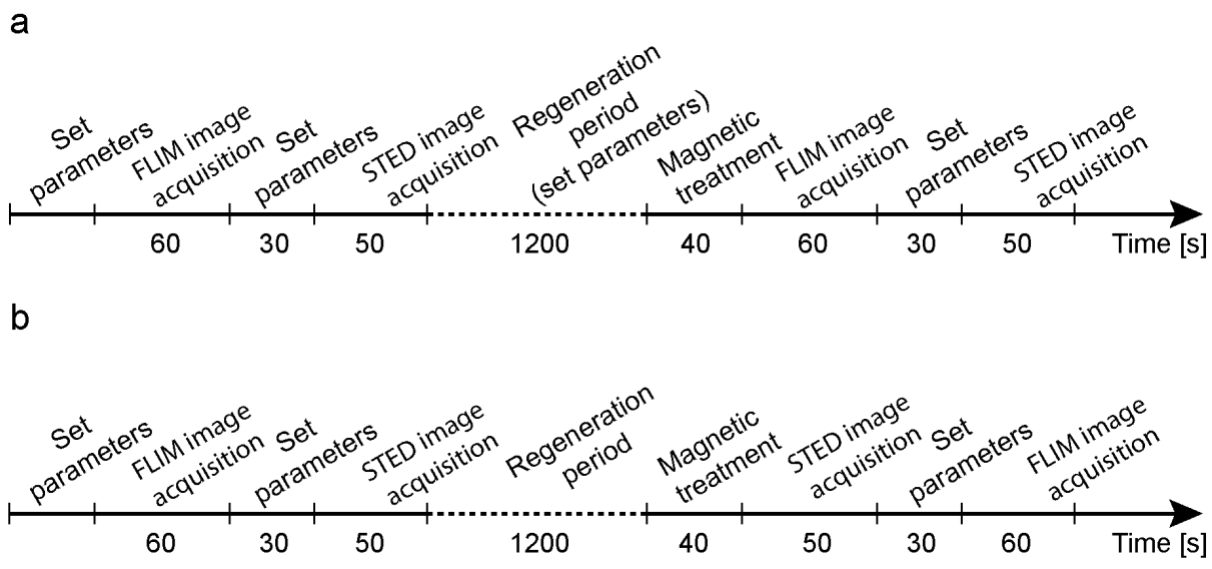

Supplementary Figure S5: **Timeline of the image acquisition.** (a) The FLIM image recording time is approx. 60 s followed by approx. 50 s for the STED imaging. In between is a short break of approx. 30 s to change the setting for the next measurement. This procedure is repeated after a 20 min regeneration period and the magnetic treatment. (b) Immediately after the regeneration period and the magnetic treatment, the STED image was recorded followed by the FLIM image acquisition.

The FRET efficiency did not change after magnetic treatment. Therefore, we changed the order of the image acquisition to reduce the time for the *de novo* synthesis of MamK.

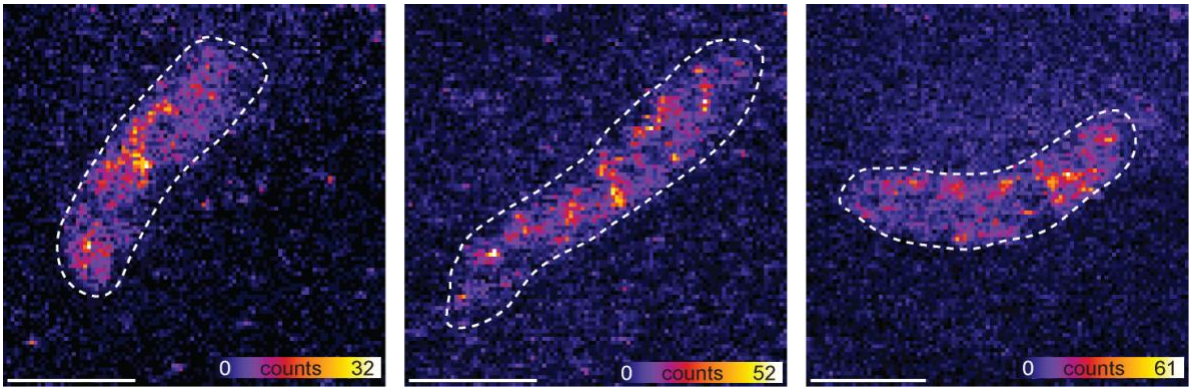

Supplementary Figure S6: **STED images of filament fragments after rotating a magnetic field and chemical fixing of the cells with 4% PFA. Scale bar: 1 µm.**

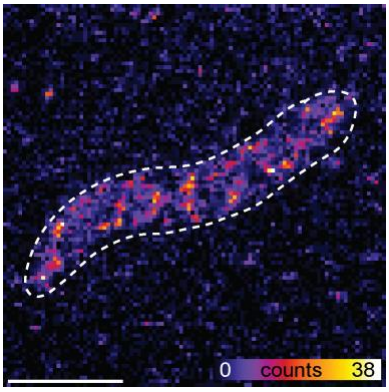

Supplementary Figure S7: **STED images of filament fragments after rotating a magnetic field and chemical fixing of the cells with 4% PFA. Scale bar: 1 µm.**

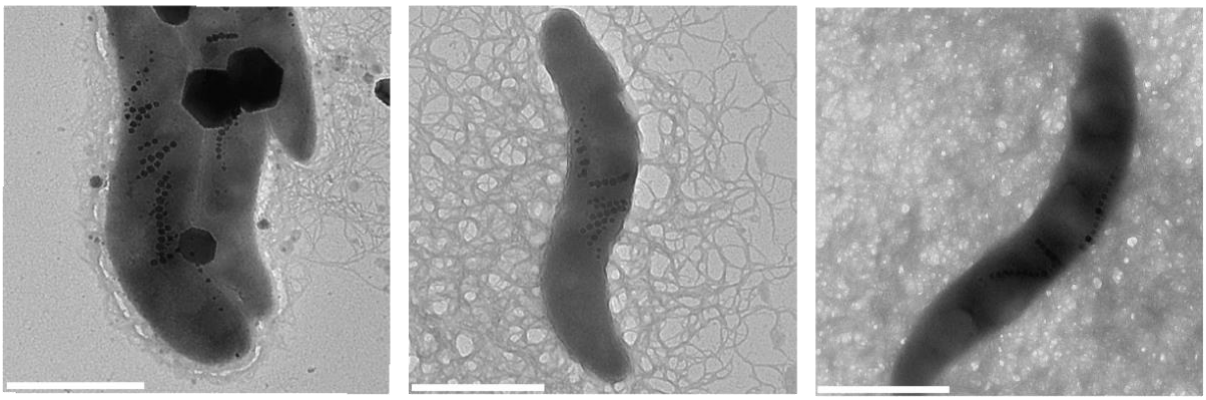

Supplementary Figure S8: **TEM images of chain fragments after rotating a magnetic field and chemical fixing of the cells with 4% PFA. Scale bar: 1 µm.**

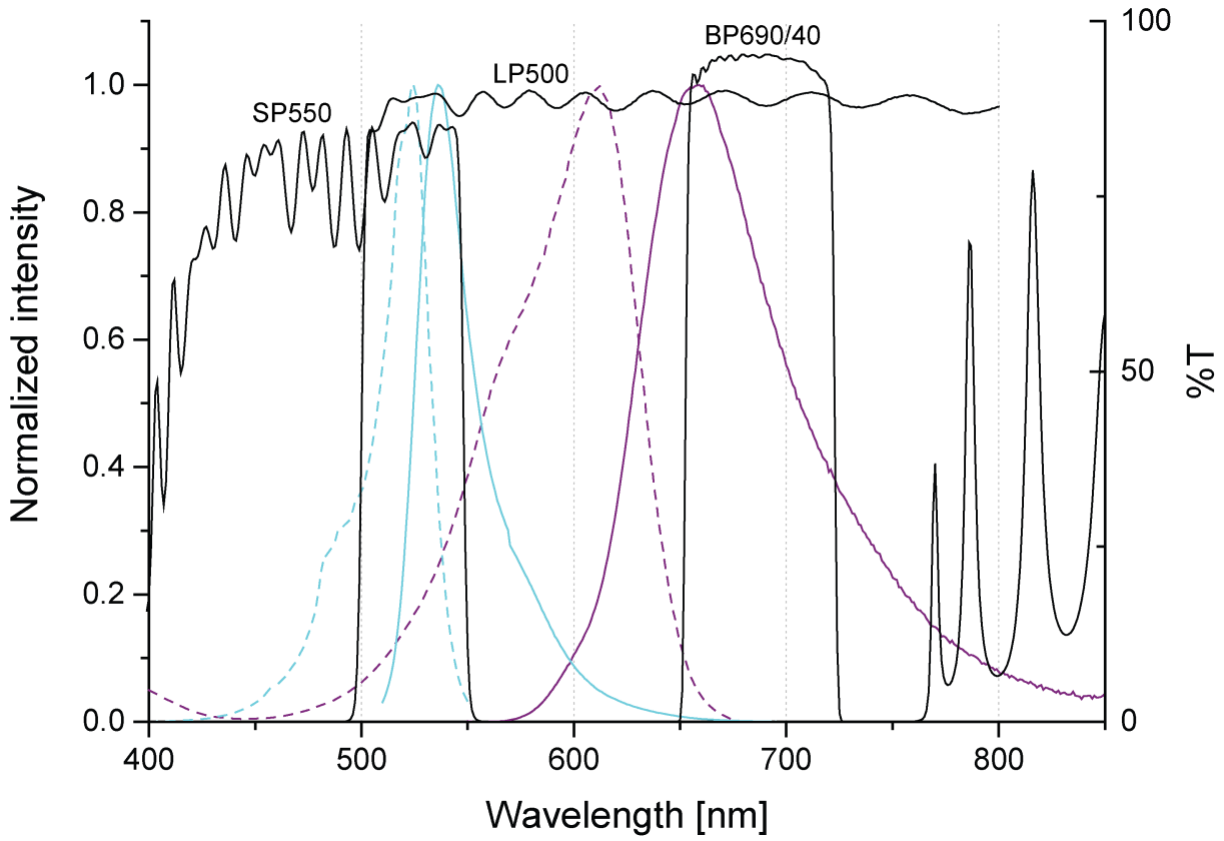

Supplementary Figure S9: **Absorption (dashed lines) and emission (solid lines) of phiYFP (cyan) and TagRFP657 (purple) as well as transmission curves of the chosen filters (black) for FLIM-FRET and STED experiments.**

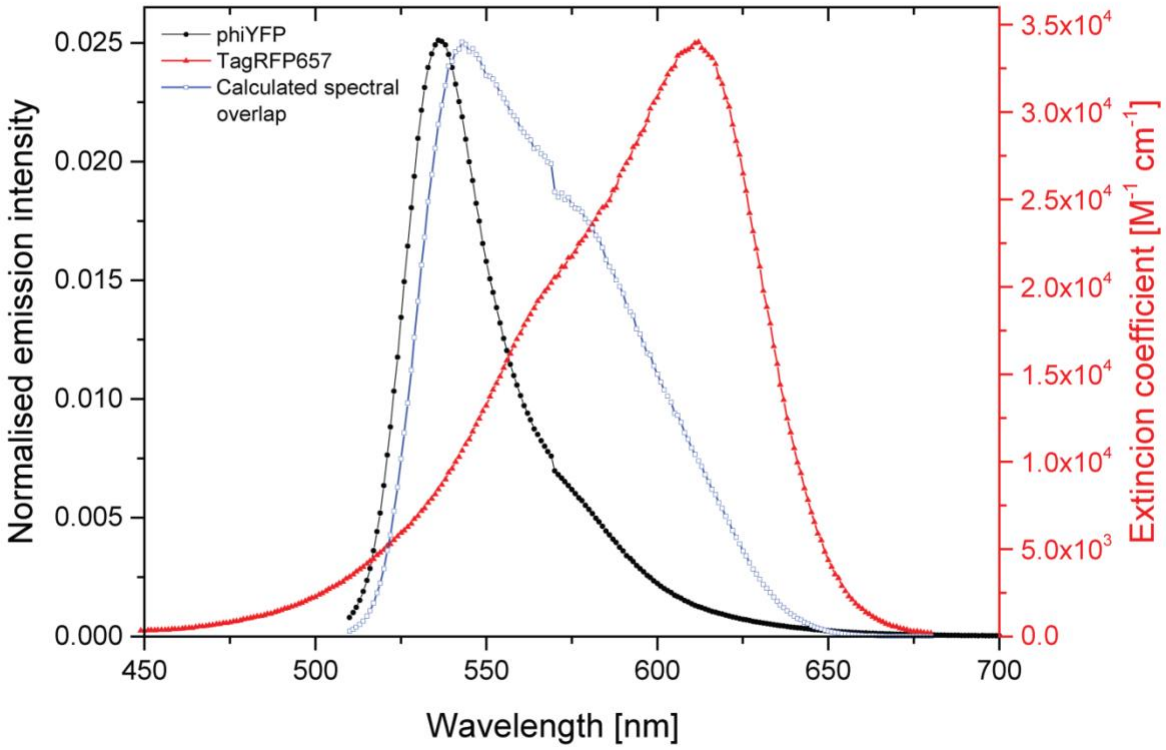

Supplementary Figure S10: **Area-normalized emission spectrum of phiYFP (black), molar absorption spectrum of TagRFP657 (red) and resulting overlap function indicating the spectral overlap integral *J(λ)*.**

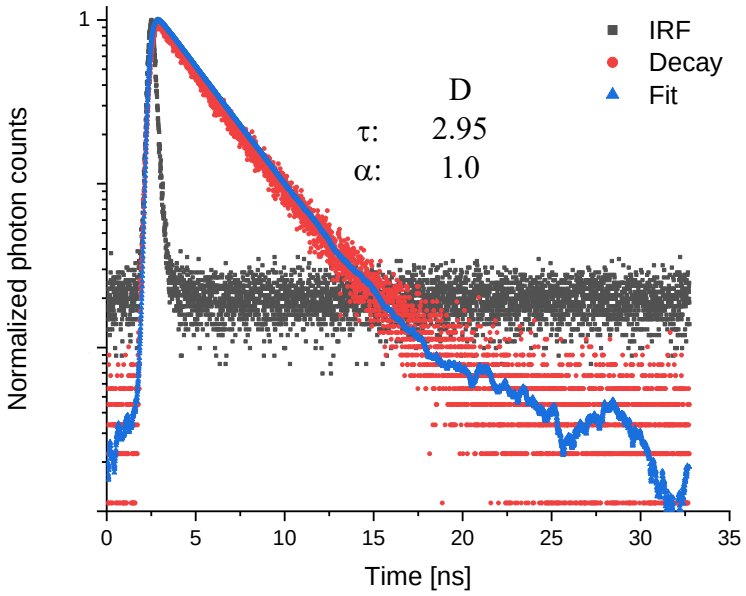

225

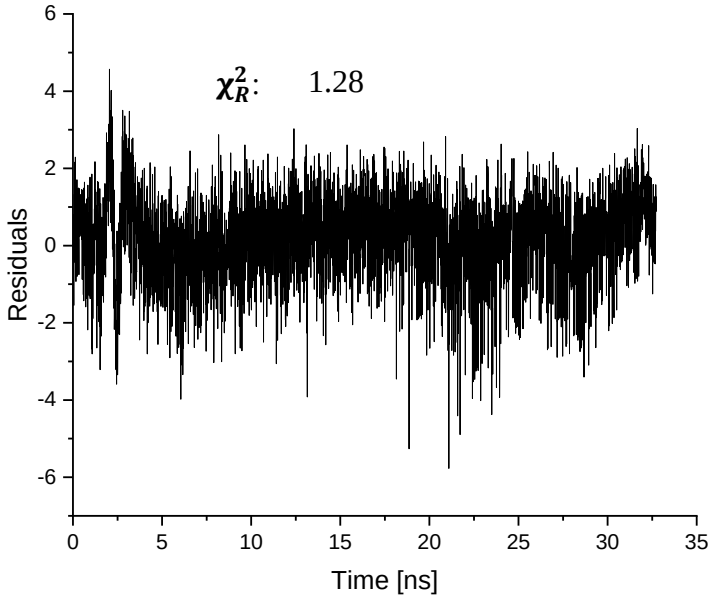

226

227 Supplementary Figure S11: ***In vivo*** **FLIM-FRET analysis in MSR-1 cells with MamJ-phiYFP**.
228 A representative phiYFP (donor) fluorescence decay curve was measured by time-correlated
229 single-photon counting (TCSPC) in MSR-1 expressing MamJ-phiYFP (red data points). For
230 MamJ-phiYFP, the data was fitted to a single-exponential deconvolution fitting model (blue),

yielding the decay time τ_D = 2.95 ns. The instrument response function (IRF) is shown in grey. The amplitude (α) is 1.0. The corresponding $\boldsymbol{\chi_R^2}$ is displayed below (1.28).

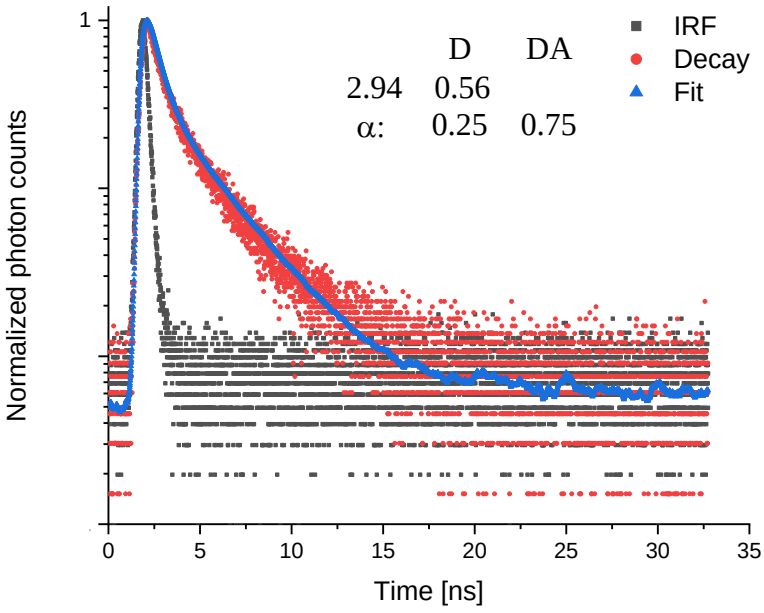

234

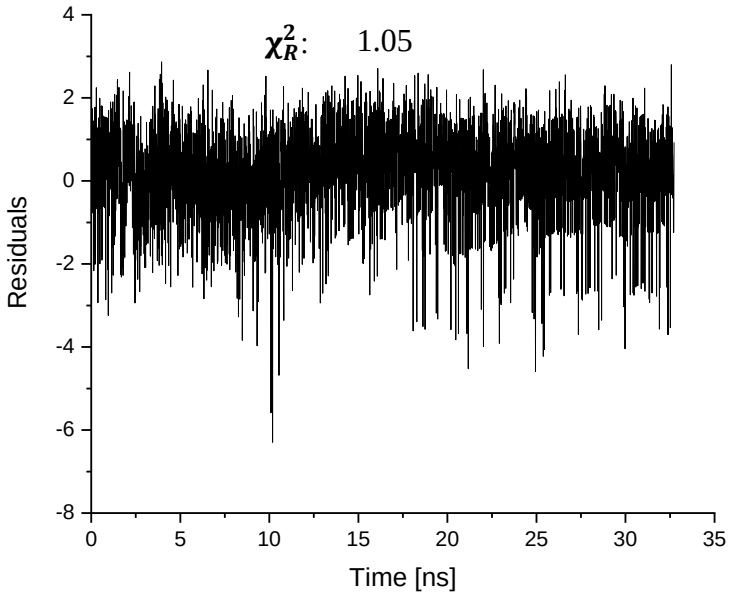

235

236 Supplementary Figure S12: ***In vivo*** **FLIM-FRET analysis in MSR-1 cells with MamJ-phiYFP**

237 **and TagFRP657-MamK**. A representative fluorescence decay curve was measured by time-

238 correlated single-photon counting (TCSPC) in MSR-1 expressing MamJ-phiYFP and TagRFP657-

MamK (red data points). The data was fitted to a bi-exponential deconvolution fitting model (blue line), yielding the decay time τ_D = 2.94 ns and an amplitude (α_D) of 0.25 along with τ_{DA} = 0.56 ns and an amplitude (α_{DA}) of 0.75. The instrument response function (IRF) is shown in grey. The corresponding $\boldsymbol{\chi_R^2}$ is displayed below (1.05).

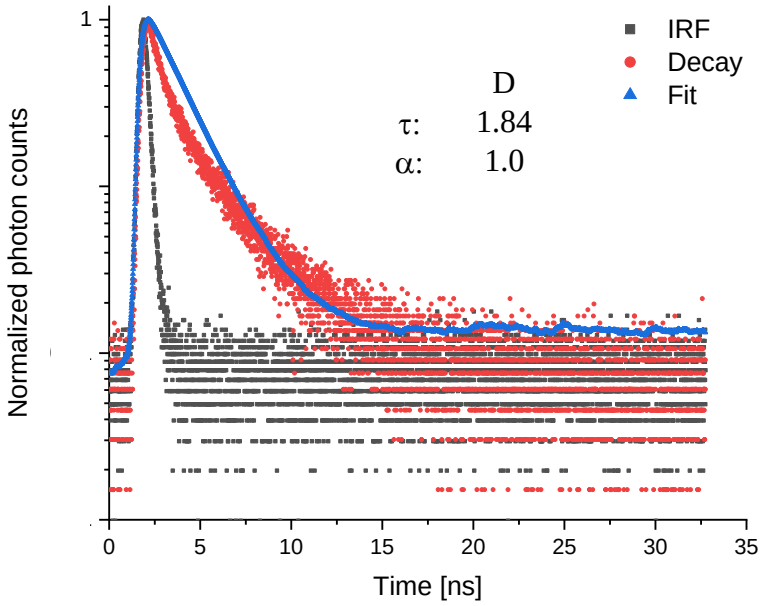

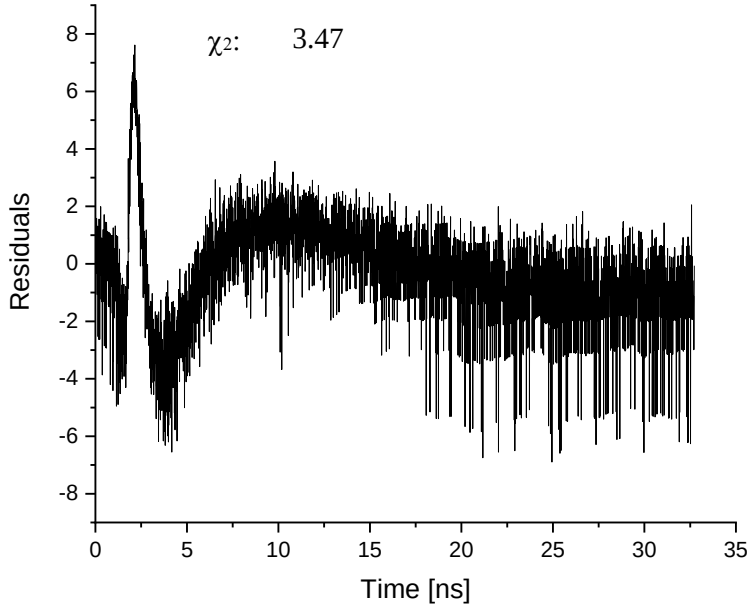

Supplementary Figure S13: ***In vivo*** **FLIM-FRET analysis in MSR-1 cells with MamJ-phiYFP and TagFRP657-MamK.** A representative fluorescence decay curve measured by time-correlated single-photon counting (TCSPC) in MSR-1 expressing MamJ-phiYFP and TagRFP657-MamK

(red data points). The data was fitted to a single-exponential deconvolution fitting model (blue line), yielding the decay time τ_D = 1.84 ns and an amplitude (α_D) of 1.0. The instrument response function (IRF) is shown in grey. The corresponding $\boldsymbol{\chi_R^2}$ is displayed below (3.47).

The fitting of the decay curve using a bi-exponential deconvolution fitting model resulted in a better χ_R^2**.** Thus we used the bi-exponential deconvolution fitting model for MSR-1 cells expressing MamJ-phiYFP and TagRFP657-MamK.

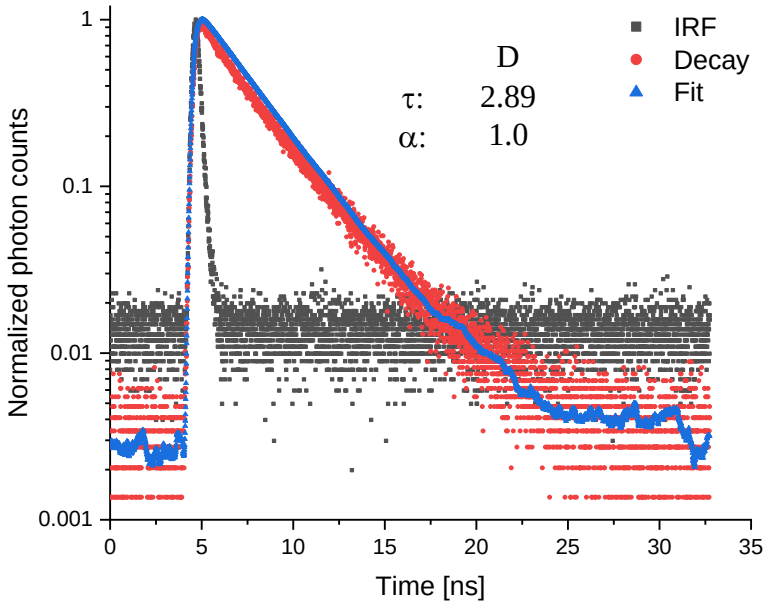

258

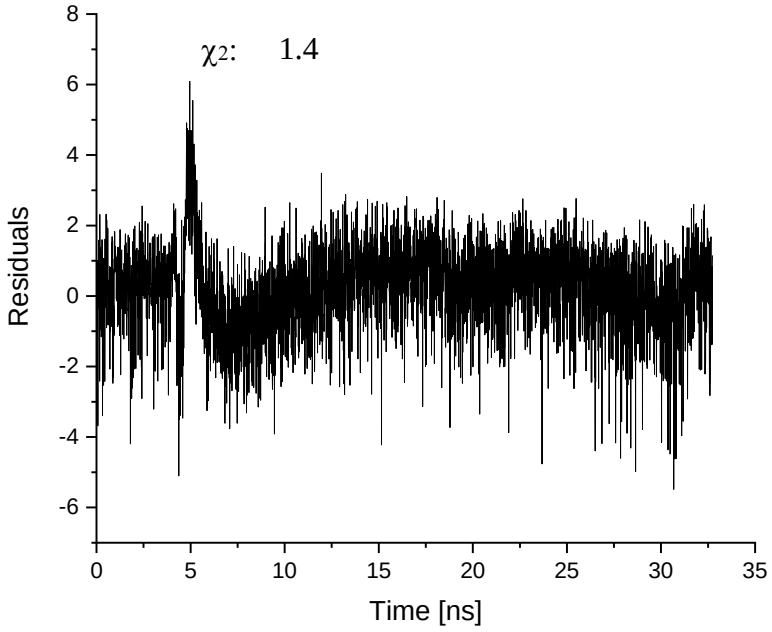

259

260 Supplementary Figure S14: ***In vivo*** **FLIM-FRET analysis in MSR-1 cells with phiYFP and**
261 **TagFRP657-MamK.** A representative fluorescence decay curves measured by time-correlated
262 single-photon counting (TCSPC) in MSR-1 expressing phiYFP and TagRFP657-MamK (red data

points). The data was fitted to a single-exponential deconvolution fitting model (blue), yielding the decay time τ_D = 2.89 ns and an amplitude (α_D) of 1.0. The instrument response function (IRF) is shown in grey. The corresponding $\boldsymbol{\chi_R^2}$ is displayed below (1.4).

Supplementary tables

Supplementary Table S1: **Full-width at half maximum (FHWM) of confocal and STED fluorescence image of TagRFP657-MamK filaments.**

Bacterium	Confocal [nm]	STED [nm]
Figure 1d	264	60
Supplementary Figure S4c	220	66
Supplementary Figure S4c	217	63
4*	233	84
5*	200	75
6*	261	54
7*	225	77
8*	202	102
9*	203	73
10*	207	80

*Images are not shown.

The FWHM was determined at the center of the cell. The mean FHWM of the confocal fluorescence images of MamK-TagRFP657 is 223 ± 23 nm and was significantly reduced to 73 ± 24 nm in STED fluorescence images ($P < 2 \cdot 10^{-7}$).

Supplementary Table S2: **Determined area of the MamK filament before and after a 20 minute regeneration period.**

Filament	I_F before magnetic treatment	I_F after magnetic treatment
Supplementary Figure S2	0.533	0.501
Supplementary Figure S2	0.369	0.366
Supplementary Figure S2	0.591	0.522
4*	0.477	0.442
5*	0.527	0.397
6*	0.49	0.491
7*	0.486	0.393
8*	0.376	0.337
9*	0.470	0.479
10*	0.446	0.429

*Images of the filaments are not shown.

Supplementary Table S3: **Fluorescence decay times of the donor phiYFP, FRET efficiencies (*E*) and donor-acceptor distances (*r*) in MSR-1 strains, together with their standard deviations (SD) as well as number of bacteria and cultures and statistical analysis.**

Constructs	τ_D ± SD [ns] ♯	τ_{DA} ± SD [ns] ♯	Statistical analysis §	*E* ± SD [%]	*r* ± SD [nm]	Bacteria	Independent cultures
MamJ-phiYFP	2.94 ± 0.07 (1.00)		n.s.			9	1
phiYFP + TagRFP657-MamK	2.97 ± 0.08 (1.00)		***			34	3
MamJ-phiYFP + TagRFP657-MamK (before mechanical treatment)	2.94 (0.27± 0.10)	0.56 ± 0.13 (0.73 ± 0.10)	***	81 ± 4	3.6 ± 0.2	72	7
MamJ-phiYFP + TagRFP657-MamK (after mechanical treatment)	2.94 (0.19 ± 0.10)	0.46 ± 0.17 (0.81 ± 0.10)	n.s.	84 ± 5	3.4 ± 0.2	45	5

♯ Mean amplitudes α_i ± SD of the respective decay time components τ_i of single- and bi-exponential decay analyses are presented in parentheses.

§ Due to non-normality (D'Agostino and Pearson omnibus normality test, P > 0.05) data were analyzed using a Kruskal-Wallis test followed by Dunn's multiple comparison tests as indicated. n.s.: non-significant, *** P < 0.001.

Supplementary Table S4: **Determined area of the MamK filament before and after applying a magnetic torque.**

Filament	I_F before magnetic treatment	I_F after magnetic treatment
Figure 3c and d	0.564	0.483
Supplementary Figure S3a and d	0.472	0.475
Supplementary Figure S4a and d	0.471	0.358
4*	0.519	0.262
5*	0.390	0.358
6*	0.317	0.270
7*	0.472	0.318
8*	0.576	0.403
9*	0.410	0.338
10*	0.380	0.341

*Images of the filaments are not shown.

Supplementary Table S5: **Bacterial strains generated and used in this study.**

Strain*	Genotype or characteristics	Reference or source
M. gryphiswaldense		
MSR WT	Wild-type MSR-1 R3/S1 (Rif_R, Sm_R).	5
Δ*mamJ*	Δ*mamJ*	6
Δ*mamK*	Δ*mamK*	7
Δ*mamJK*	Δ*mamJK*	4
MamJ-phiYFP	MSR WT, conjugated with pMT092, Km_R	This work
TagRFP657-MamK	MSR WT, conjugated with pMT094, Km_R	This work
MamJ-phiYFP + TagRFP657-MamK	MSR WT, conjugated with pMT095, Km_R	This work
phiYFP + TagRFP657-MamK	MSR WT, conjugated with pMT107, Km_R	This work
phiYFP	MSR WT, conjugated with pMT108, Km_R	This work
Δ*mamJ* + MamJ-phiYFP	Δ*mamJ*, conjugated with pMT092, Km_R	This work
Δ*mamK* + TagRFP657-MamK	Δ*mamK*, conjugated with pMT094, Km_R	This work
Δ*mamJK* + MamJ-phiYFP + TagRFP657-MamK	Δ*mamJK*, conjugated with pMT095, Km_R	This work
E. coli		
DH5α	Host for cloning. F- φ80*lacZ*ΔM15 Δ(*lacZYA-argF*) U169 *rec*A1 *end*A1 *hsd*R17 (rK-, mK+) *pho*A *sup*E44 λ-*thi*-1 *gyr*A96 *rel*A1	Invitrogen
WM3064	Host for cloning and conjugation. *thrB1004 pro thi rpsL hsdS lacZ*ΔM15 *RP4-1360* Δ(*araBAD*)*567* Δ*dapA1341*::[*erm pir* (*wt*)]	W. Metcalf, (unpublished)

293 Supplementary Table S6: **Plasmids generated and used in this study.**

Plasmid	Relevant characteristics	Reference or source
pBBR1-MCS2	Replicative backbone vector for *in trans* gene expression in MSR. *ori*T, mob, Km_R	[8]
pMT080	pBBR1-MCS2 based vector, Km_R, P_{mamAB}-*α-helix* (linker)	[4]
pMT082	pBBR1-MCS2 based vector, Km_R, P_{mamAB}-*mamJ-dendra2*	[4]
pMT092	pMT082 derivative, P_{mamAB}-*mamJ-phiYFP*	This work
pMT093	pMT080 derivative, P_{mamAB}-*RFP657*-linker	This work
pMT094	pMT093 derivative, P_{mamAB}-*TagRFP657-mamK*	This work
pMT095	pMT092 derivative, P_{mamAB}-*mamJ-phiYFP_TagRFP657-mamK*	This work
pMT107	pMT095 derivative, P_{mamAB}-*phiYFP_TagRFP657-mamK*	This work
pMT108	pMT107 derivative, P_{mamAB}-*phiYFP*	This work

294

295 Supplementary Table S7: **Oligonucleotides used in this work.**

Name	Sequence 5'→3'	Remarks
oMTN045	agacta**GGATCC**TCACTGACCGGAAACGTCACCAAGC	Overhang, *Bam*HI
oMTN292	agacta**AAGCTT**ATGAGCAGCGGCGCCCTGCT	Overhang, *Hind*III
0MTN293	agacta**GGATCC**TCACAGGTAGGTCTTGCGGCAATCC	Overhang, *Bam*HI
oMTN294	agacta**CATATG**AGCGAGCTGATTACCGAGAACATGC	Overhang, *Nde*I
oMTN295	agacta**GAATTC**ATTCAGCTTGTGCCCCAGTTTGCTAGG	Overhang, *Eco*RI
oMTN296	agacta**AAGCTT**ATGAGTGAAGGTGAAGGCCAGGCC	Overhang, *Hind*III
oMTN297	agacta**GGATCC**ctgacccttgaattaaggacaacagcgATGAGCGAGCTGATTACCGAGAACATGC	Overhang, *Bam*HI, Lowercases: *mamC* intergenic region
oMTN298	agacta**CTCGAG**TCACTGACCGGAAACGTCACCAAGCTG	Overhang, *Xho*I
oMTN353	agacta**CATATG**AGCAGCGGCGCCCTGCT	Overhang, *Nde*I
oMTN355	agacta**CTCGAG**TCACTGACCGGAAACGTCACCAAGC	Overhang, *Xho*I

296

297 **References**

298 1. Becker, W. Fluorescence lifetime imaging--techniques and applications. *J. Microsc.* **247,**
299 119–36 (2012).

300 2. Jahn, K., Buschmann, V. & Hille, C. Simultaneous Fluorescence and Phosphorescence
301 Lifetime Imaging Microscopy in Living Cells. *Sci. Rep.* **5,** 14334 (2015).

302 3. Wahl, M. & Orthaus-Müller, S. Time tagged time-resolved fluorescence data collection in
303 life science. *Tech. note, PicoQuant GmbH* (2014).

304 4. Toro-Nahuelpan, M. *et al.* Segregation of prokaryotic magnetosomes organelles is driven
305 by treadmilling of a dynamic actin-like MamK filament. *BMC Biol.* **14,** 88 (2016).

306 5. Schultheiss, D. & Schüler, D. Development of a genetic system for Magnetospirillum
307 gryphiswaldense. *Arch. Microbiol.* **179,** 89–94 (2003).

308 6. Scheffel, A. *et al.* An acidic protein aligns magnetosomes along a filamentous structure in
309 magnetotactic bacteria. *Nature* **440,** 110–114 (2006).

310 7. Katzmann, E., Scheffel, A., Gruska, M., Plitzko, J. M. & Schüler, D. Loss of the actin-like
311 protein MamK has pleiotropic effects on magnetosome formation and chain assembly in
312 Magnetospirillum gryphiswaldense. *Mol. Microbiol.* **77,** 208–224 (2010).

313 8. Kovach, M. E., Phillips, R. W., Elzer, P. H., Roop, R. M. & Peterson, K. M. pBBR1MCS:
314 a broad-host-range cloning vector. *Biotechniques* **16,** 800–2 (1994).

315